Desalination and Water Treatment
www.deswater.com
doi: 10.5004/dwt.2022.28553

262 (2022) 27–37
June

Performance modelling of direct contact membrane distillation for flat sheet module

Karim Choubani*, Mariem Sammoudi, Ridha Ennetta

Research Unit: Mechanical Modeling, Energy & Materials (M²EM), UR17ES47, National Engineering School of Gabes (ENIG), Avenue Omar Ib-Elkhattab, 6023, Zrig, Gabes, Tunisia, Tel. (216) 97310335/(216) 52537209/(216) 98 487 430; emails: chambanik@yahoo.fr (K. Choubani), mariemlfgm@gmail.com (M. Sammoudi), ridha_ennetta@yahoo.fr (R. Ennetta)

Received 7 December 2021; Accepted 9 May 2021

ABSTRACT

The main objective of this paper is to develop a general predictive mathematical model of direct contact membrane distillation (DCMD) for flat sheet module. This model, based on fundamental equations of mass and heat transfer, aims to predict the water permeate flux across the membrane and to investigate the influence of membrane characteristics such as its thickness, its length, the pore size and porosity, on the performance of DCMD process. All physical parameters implemented in the mathematical model have been estimated using appropriate temperature correlations. Obtained results revealed that doubling the thickness of the membrane decreases the permeate flux by an amount of 43% and increasing the membrane porosity by 20% yields an increase of the permeate flux by 40%. However, pore size as well as membrane length variations show no sensitive effect on permeate flux. A good agreement between this theoretical model and experimental data was observed for various feed temperatures. This suggests that this tool could be utilized efficiently to predict permeate flux values for DCMD process.

Keywords: Heat and mass transfer; Direct contact membrane distillation; Flux prediction; Modeling; Membrane characteristics

1. Introduction

In the case of direct contact membrane distillation, the transmembrane partial pressure difference is generated by a temperature difference between the hot water feed and a cold water collecting the permeate on either side of the hydrophobic membrane. The volatile molecules thus evaporate at the hot water/vapor interface, pass through the membrane in gaseous form before being recondensed at the vapor/cold water interface. Recondensation, thus, takes place inside the membrane module.

Schofield et al. [1–3] is the first who proposed a heat and mass transfer mathematical model of direct contact membrane distillation (DCMD) for flat sheet module. This model considers the viscous flow, the Knudsen diffusion and the ordinary diffusion and gives a good control and optimization features for basic study of DCMD. Tomaszewska et al. [4] presented a 1-D mathematical model of DCMD for flat sheet module. In that model, authors estimated the temperatures and concentrations of the feed and permeate flows along the DCMD unit. Laganà et al. [5] applied a model on cylindrical geometry fiber DCMD modules. In that model, the flow regime of the feed and permeate liquids and the operation steady state were determined. Ding et al. [6] proposed a model based on nonlinear regression to evaluate the membrane distillation coefficient in three different kinds of membrane. They showed that theoretical results agree well with experimental data.

Phattaranawik et al. [7] proposed a heat and mass transfer model. This model was used to identify the meaning of each heat transfer mechanism and the effect of mass transport on heat transfer rates.

* Corresponding author.

Yuna et al. [8] proposed a model, which takes into account the effect of fouling resistance, membrane resistance and concentration polarization on permeate flux. Authors obtained good agreement between predictions and experimental results.

Qtaishat et al. [9] proposed a mathematical model using MATLAB simulation. This model is based on values of the feed solution temperatures and the mass fluxes obtained experimentally. They showed that the mass transport contribution to the total transferred heat was small in both feed and permeate boundary layers. While, it was important in the membrane region.

Yu et al. [10] and Yang et al. [11] presented a computational fluid dynamics (CFD) method in the hollow fiber DCMD modelling. They simulated only one membrane contained in the hollow fiber module. In that model, Yu et al. [10] and Yang et al. [11] described the momentum balance and they estimated the velocity, concentration and temperature profiles in the feed and permeate sides in a hollow fiber DCMD module. They also, determined the total values for the heat and mass transport through the membrane.

Andrjesdóttir et al. [12] proposed a dusty gas model for mass transport to compare experimental results with predicted ones, in the case of feed solution with high NaCl concentration. In that model, they showed that for a flat sheet membrane module the combined Knudsen-molecular diffusion was the best mode to calculate the permeate flux.

Lawal and Khalifa [13] proposed an iterative model to predict the permeate flux. They showed that permeate flux increases with increasing pore size up to a critical value where permeate flux remains constant.

Hayer et al. [14] proposed another model based on the CFD. In that model, in each point of the hollow fiber DCMD module the velocity and concentration profiles are determined while the temperature variations are presented for the feed and permeate sides and the heat transfer through the membrane is not simulated. Bouchrit et al. [15] proposed an operative model to measure the permeate flux predicted by the Knudsen-molecular mechanism model. They showed experimentally the ability to treat high saline solution by using DCMD process.

Gustafson et al. [16] proposed a stepwise model in which the hollow fiber and flat sheet DCMD unit is decomposed into numerous parts. For each part, the mass and heat balances are determined. This model is very adequate to optimize the length of DCMD modules. Eleiwi et al. [17] proposed a model based on dynamic operation of flat sheet DCMD module. In this model, they used 2D advection-diffusion equations to analyze the heat and mass transport within the DCMD unit. The temperature profiles within the feed and permeate domains were fully described by this model. However, for the membrane field, the temperature and concentration of the water vapor were not fully estimated. Cheng et al. [18] proposed a model based on the methodology of the response surface. This methodology was based on experimental connections between controlled variables and response variables. This model is based on the interaction between the optimization variables such as the inlet temperatures of the feed and permeate flows, the velocity of the feed fluid, the module packing density and the length-diameter ratio and the response objectives such as the permeate flux, the water production, per energy consumption and per unit volume of module.

Patil et al. [19] proposed a model based on MATLAB simulation to predict the permeate flux. In that model, the influence of operational parameters on the permeate flux were studied.

Ali et al. [20] proposed a model based on a many partition of the hollow fiber and flat sheet DCMD module. For each section, the heat and mass balances are determined and the polarization temperature is well estimated. Ali and Orfi [21] proposed a theoretical model based on heat and mass transport balances. In that model, the effect of inlet feed temperature and flow rate on permeate flux was experimentally studied. Obtained results were used to calibrate the theoretical model.

Lou et al. [22] proposed an experimentally validated two-dimensional CFD code that simulates heat and mass transfer in a 2-D flat sheet DCMD system. In that model, coupled temperature and concentration, polarization in the DCMD process, used to treat brines with high salinity, is studied.

Ni et al. [23] suggested a simulation model coupling heat and mass transport in a 2-D horizontal flat sheet membrane surface via a user-defined function program. In that model, they studied the optimal membrane thickness and they showed that the counter-current operation mode was better than co-current operation. Alqsair et al. [24] conducted CFD simulations in a 3-D dimensional MD module to determine the steady-state velocity, temperature, and concentration field in the feed and permeate sides. In that model, they showed that the local variation of vapor flux, temperature polarization and concentration polarization characteristics change with changing the module length in the sweeping gas membrane distillation (SGMD) systems but does not modify the local behavior in DCMD systems.

Mohammad Ameen et al. [25] developed a model by using a system of nonlinear equations solved numerically by MATLAB software. They showed that the rise in feed temperature and flow rate increase the permeate flux across the membrane, while the increase of the feed concentration decrease the permeate flux. The simulation results showed that the appearance of extra mass transfer resistance varied with varying the feed temperature and concentration.

Ve et al. [26] studied experimentally and numerically the effect of spacers and operating conditions on mass transfer characteristics in DCMD systems. They proposed a procedure to examine the effect of feed inlet temperature, feed concentration, and velocity on the mass transport coefficient, the boundary layer thickness and the shear stress, and flow properties in spacer-filled channels of DCMD systems. They showed in their results that the plastic spacer (PL4) was suggested to be the most effective to enhance mass transfer properties.

The present study focused on direct contact membrane distillation performance with different membrane characteristics. The membrane characteristics tested numerically were the thickness, the pore size, the porosity, and the length. Theoretical results were performed at different feed temperatures and constant cold inlet temperatures, and vapor fluxes for different operating conditions were analyzed. The predicted mathematical model was

developed to evaluate the performance of DCMD for a flat sheet module.

2. Modelling and configuration description

In DCMD process, transport of heat and mass occurs simultaneously. Water vapor molecules cross the membrane without wetting its pores. The hydrophobicity of membranes does not allow water to cross membrane pores unless the transmembrane pressure surpasses the liquid entry pressure (LEP). In current modelling the system is as described in Fig. 1. It consists of hot-water compartment and cold-water compartment separated by a hydrophobic porous membrane material. The hot temperature T_h decreases over the feed side to T_{mh} at the membrane surface. The cold water temperature T_c increases across the cold layer to T_{mc} at the membrane surface to the cold side as vapour condenses into the fresh water. The driving force is hence the vapour pressure difference between hot and cold membrane surfaces.

2.1. Modelling assumptions

Some assumptions required to simplify the 1-D performance model of direct contact membrane distillation for flat sheet module:

- The system was isolated, thermal losses to the environment are negligible.
- The effect of salt concentration is not taken into account.
- 1-D heat transfer, the temperature variation across the second dimension (the width) of the membrane is neglected.
- Sensible heat transferred by the permeate is neglected.

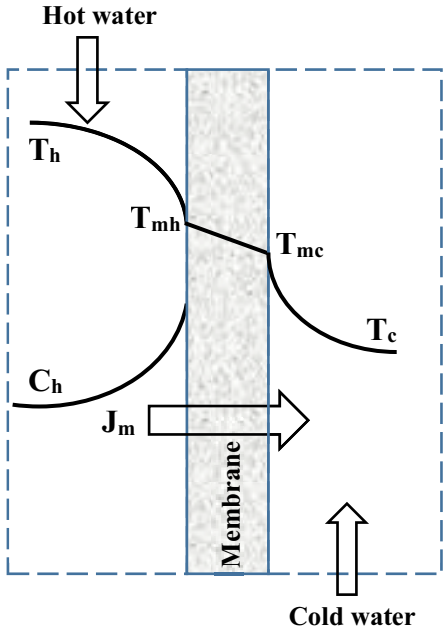

Fig. 1. Temperature and concentration variations in a single layer hydrophobic membrane used in DCMD process.

2.2. Mass transfer

Mass transfer is a transfer of vapor from the hot to the cold-water side where it condenses. In the case of DCMD, mass transfer is due to three modes (or three mechanisms) of diffusion:

- *Knudsen diffusion*: which is related to the collision of molecules on the surface of the membrane. This mode of diffusion is realized when the Knudsen number $K_n > 10$.
- *Molecular diffusion*: which is related to the intermolecular collision. This mode of diffusion is carried out when the Knudsen number $K_n < 0.01$.
- Combined Knudsen – molecular diffusion or so-called transient region is carried out for Knudsen number $0.01 < K_n < 10$

The Knudsen number is a function of the pore diameter and it is defined by the following expression:

$$K_n = \frac{K_B \dfrac{T_{mav}}{\sqrt{2}\cdot\pi\cdot P_a\left(2.641\times10^{-10}\right)^2}}{d_p} \tag{1}$$

where K_B = 1.381 × 10^{-23} J K^{-1} is the Boltzmann constant, P_a is the mean pressure within the membrane pores, $T_{mav} = T_{mh} + T_{mc}/2$ is the absolute mean temperature in the pores.

2.2.1. Mass transfer model

The mass flux J_m, depends on the difference in partial vapor pressure of hot and cold liquids on both sides of the membrane and on the coefficient of the membrane (equivalent to the diffusion coefficient). It is given by the following expression:

$$J_m = B_m\left(P_{mh} - P_{mc}\right) \tag{2}$$

where B_m is the characteristic coefficient of the membrane, P_{mh}, P_{mc} are the partial vapor pression respectively in the hot side and in the cold one. For pure water P_{mh}, P_{mc} are determined by Antoine's equation, which relates these pressures to the temperatures of the membrane surface as follows:

$$P_{mh} = \exp\left[\left(23{,}1964\right) - \frac{3816{,}44}{T_{mh} - 46{,}13}\right] \tag{3}$$

$$P_{mc} = \exp\left[\left(23{,}1964\right) - \frac{3816{,}44}{T_{mc} - 46{,}13}\right] \tag{4}$$

where T_{mh} is the average membrane surface temperature on the hot water side and T_{mc} is the average membrane surface temperature on the cold water side.

2.2.2. Diffusion coefficient (or characteristic coefficient) of the membrane B_m

- In the case of Knudsen diffusion ($K_n > 10$) the coefficient B_m is given by the following expression:

$$B_m = \frac{\varepsilon \cdot d_p}{3 \cdot \tau \cdot \delta} \sqrt{\frac{8 \cdot M_w}{\pi \cdot R \cdot T_{\text{mav}}}} \tag{5}$$

- In the case of molecular diffusion ($K_n < 0.01$) the coefficient B_m is given as following:

$$B_m = \frac{\varepsilon \cdot \text{PD} \cdot M_w}{\tau \cdot \delta \cdot P_a \cdot R \cdot T_{\text{mav}}} \tag{6}$$

- Theoretical and experimental studies showed that the combined Knudsen-molecular diffusion is the most efficient and closest to reality. In our study, we therefore adopted this mode of diffusion. In this region, the coefficient B_m is given by the following expression:

$$B_m = \left[\frac{\varepsilon \cdot \tau \cdot \delta}{\varepsilon \cdot \text{d}_p} \sqrt{\frac{\pi \cdot R \cdot T_{\text{mav}}}{8 \cdot M_w}} + \frac{\tau \cdot \delta \cdot P_a \cdot R \cdot T_{\text{mav}}}{\varepsilon \cdot \text{PD} \cdot M_w} \right]^{-1} \tag{7}$$

where R is the ideal gas constant (R = 8.314 J mol^{-1} K^{-1}), M_w is molecular mass of water molecules.

The diffusivity of water vapors (P.D) through the static air in the membrane is calculated by the following expression (Pa m^2 s^{-1}):

$$\text{P.D} = 1{,}895 \times 10^{-5} T_{\text{mav}}^{2{,}072} \tag{8}$$

2.3. Heat transfer

Heat transfer in a DCMD module occurs in three regions:

- The convective flow $Q_{\text{conv},h}$, transported by the hot water to the surface of the membrane is given by Newton's law:

$$Q_{\text{conv},h} = h_h \left(T_h - T_{m,h} \right) \tag{9}$$

where h_h is the convective transfer coefficient on the hot water side determined from the correlations according to the type of laminar or turbulent flow.

- The heat produced by the vapors Q_v, (evaporative heat transfer) is given by the following expression:

$$Q_v = J_m \times L_v \tag{10}$$

where L_v is the latent heat of vaporization (enthalpy of vaporization), given by the following expression:

$$L_v = \left[\left(1{,}7535 \times T_{\text{mh}} \right) + 2024{,}3 \right] \tag{11}$$

Fourier's law gives the conductive flux Q_c through the membrane:

$$Q_c = \left(\frac{K_m}{\delta} \right) \cdot \left(T_{\text{mh}} - T_{\text{mc}} \right) \tag{12}$$

where K_m is the membrane effective conductivity, given by the following equation:

$$K_m = \left[\left(\frac{\varepsilon}{K_g} \right) + \left(\frac{1-\varepsilon}{K_p} \right) \right]^{-1} \tag{13}$$

Thus, the total flux transferred through the membrane is equal to:

$$Q_m = Q_v + Q_c \tag{14}$$

On the other side of the membrane (cold side), the convective heat flow transported from the cold surface of the membrane to the permeate is given by Newton's law:

$$Q_{\text{conv},c} = h_c \left(T_{\text{mc}} - T_c \right) \tag{15}$$

In steady state, the energy conservation is validated and we obtain the following equality:

$$Q_{\text{conv},h} = Q_m = Q_{\text{conv},c} \tag{16}$$

From this equality, we can determine an analytical solution of the membrane surfaces temperatures T_{mh} and T_{mc}:

$$T_{\text{mh}} = T_h - \frac{Q}{h_h} \tag{17}$$

$$T_{\text{mc}} = T_c + \frac{Q}{h_c} \tag{18}$$

and

$$Q = \left(\frac{1}{\left(\frac{1}{h_h} + \frac{1}{h_m + \left[J_m L_v \Big/ \left(T_{\text{mh}} - T_{\text{mc}} \right) \right]} + \frac{1}{h_c} \right)} \right) \left(T_h - T_c \right) \tag{19}$$

where

$$U = \frac{1}{\frac{1}{h_h} + \frac{\delta}{K_m} + \frac{1}{h_c}} \tag{20}$$

2.4. Coupling between mass and heat transfer

The following equation gives the convective heat transfer coefficient *h*:

$$h_i = \frac{N_u \times K_i}{d_{h,i}} \tag{21}$$

where $i = h$ (hot) or c (cold); Nu is the Nusselt number; K is the mean thermal conductivity; d_h is the hydraulic diameter of the channel

The Nusselt number is given as a function of the Reynolds number and the Prandtl number (Table 1).

The Prandtl number P_r is given by the following equation:

$$P_r = \frac{\nu_i}{\alpha_i} = \frac{\mu_i \cdot C_{p,i}}{K_i} \tag{22}$$

where μ is the dynamic viscosity and α_i is the thermal diffusivity

The Reynolds number, characterizing the flow regime, is given as follows:

$$R_e = \frac{v_i \cdot d_{h,i}}{\nu_i} = \frac{\rho \cdot v_i \cdot d_{h,i}}{\mu_i} \tag{23}$$

where v is mean velocity and ρ is the density.

3. Numerical simulation

To predict the permeate flux production, a code was developed and implemented in MATLAB. The thermodynamic, transport and physical properties of water were calculated based on correlations reported in Table 2. For DCMD process, measurements of the membrane surface

Table 1
Numerical correlations used to calculate Nusselt number in the case of laminar and turbulent flow regime

Correlations	Flow regime	References
$\mathrm{Nu} = 1.86\left(\frac{\mathrm{Re}\cdot\mathrm{Pr}}{L/d_h}\right)^{1/3}$ (24)	Laminare	[27]
$\mathrm{Nu} = 0.023\left(1+\frac{6d_h}{L}\right)\mathrm{Re}^{0.8}\mathrm{Pr}^{1/3}$ (25)	Turbulent	[28]

Table 2
Physical properties of correlations

Physical property	Correlations	Regression coefficients	References
Density (g mL^{-1})	$AB^{-\left(1-\frac{T}{T_c}\right)^n}$	$A = 0.34710$ $B = 0.27400$ $n = 0.28571$ $T_c = 374$°C	[29]
Water viscosity (Pa·s)	$\log_{10}\mu = \frac{A+B}{T+CT+DT^2}$	$A = -10.21158$ $B = 1.7925 \times 10^{-3}$ $C = 1.7730 \times 10^{-2}$ $D = -1.263 \times 10^{-5}$	[29]
Air viscosity (Pa·s)	$A + BT + CT^2$	$A = 9.1445$ $B = 0.029257$ $C = 0.000019067$	[29]
Thermal capacity (J mol^{-1} K^{-1})	$A + BT + CT^2 + DT^3$	$A = 92.053$ $B = 3.9953 \times 10^{-2}$ $C = -2.1103 \times 10^{-4}$ $D = 5.3469 \times 10^{-7}$	[29]
Latent heat of vaporization (kJ mol^{-1})	$A + BT + CT^2 + DT^3$	$A = 2327.3$ $B = 1.4317$ $C = 0.010953$ $D = 1.2365 \times 10^{-5}$	[30]
Thermal conductivity (W mK^{-1})	$A + BT + CT^2$	$A = 0.2758$ $B = 4.6120 \times 10^{-3}$ $C = -5.5391 \times 10^{-6}$	[29]

temperatures were not possible. An iterative approach was carried out by simultaneously solving the heat and mass transfer equations to compute the surface temperatures of the membrane and then deduce the permeate flux.

Initially the temperature values of the hot and cold surfaces of the membrane are estimated to be equal to the inlet temperatures of the hot and cold water (i.e., initially $T_{mh0} = T_{h0}$ and $T_{mc0} = T_{c0}$). These values of temperatures are used to calculate the vapor pressures P_{mh} and P_{mc}, then estimate the permeate flow J_m. The value (T_{mh}) is then decremented by a value equal to Q/h_h and the value of (T_{mc}) is incremented by a value equal to Q/h_c. The new values of T_{mh} and T_{mc} are used to estimate a new value of the permeate flux J_m. The above procedures were repeated until the maximum difference between two consecutive values of the temperatures T_{mh} and T_{mc} is less than 0.1%. The flowchart of Fig. 2 depicts the multistep procedure adopted to solve heat and mass transfer equations:

4. Results and discussions

In the current work, the influences of membrane characteristics on the permeate flux in pure water solution have been simulated and analyzed. The effects of thickness (δ), pore size (d_p), porosity (ε) and membrane length (L) have been studied. The optimal membrane physical characteristics were deduced for different operation conditions.

4.1. Model validation

To validate our calculation code with experimental results, we used the same membrane properties and geometrical constant presented by Andrjesdóttir et al. [12] in their experiments (Table 3)

This validation was achieved for a hot water (feed) temperature varying from 45°C to 65°C, constant cold water temperature equal to 20°C, feed flow equal to 12 L min^{-1} and permeate flow equal to 4 L min^{-1}.

Fig. 3 shows the validation of our calculation code. Obtained results demonstrate the correlation between the experimental data (red points) obtained by Andrjesdóttir et al. [12] and the simulated results (black points) and the corresponding goodness of fit (relative error does not exceed 5%). Obtained results are in very good agreement too with theoretical data obtained by Lawal and Khalifa [13]. The results of the DCMD simulations demonstrate that a rise in the feed temperature leads to an increase in the permeate flux. The feed temperature rise increases the partial pressure of the water vapor at the feed-membrane interface and therefore improves the driving force of the process.

Obtained results showed that the rise in the feed temperature from 45°C to 65°C leads to 3.3-fold increase in the vapor flux.

4.2. Effect of the membrane thickness

In these experiences, feed temperature (T_h) varying from 45°C to 65°C and permeate temperature (T_c) is considered constant and equal to 20°C.

Fig. 4 shows the temperature variation of the permeate-membrane interface (T_{mc}), with the membrane thickness (δ). Obtained results show that, doubling the membrane thickness δ leads to approximately 12% fold decrease in the permeate surface temperature T_{mc}. This decrease is due to the reduction of the conductive flux Q_c through the membrane.

Fig. 5 shows that the thickness increase of the membrane leads to an increase in the temperature of the feed-membrane interface. In fact, doubling the thickness of the membrane produces an increase in the feed-membrane temperature around 2%. However, thickness rise decreases the temperature of the permeate-membrane and has the direct proportional effect on the temperature of the feed-membrane interface. This effect is due to the thermal resistance layer which forms adjacent to the membrane surface due to the presence of the temperature boundary layer resistance further reduces the transmembrane vapor flux.

Fig. 6 shows that doubling the membrane thickness leads to almost 15% increase in the difference temperature across the membrane interfaces.

Although membranes generally have low thermal conductivity, the temperature difference between the feed and permeate sides (driving force) for mass transfer will also lead to significant conductive heat transfer through the membrane due to the effect of the membrane thickness.

Fig. 7 shows that (i) the water vapor flux decreased by a value of 43% with the increase in the membrane thickness from 100 to 200 μm. This value (43%) remains constant for a fixed permeate temperature equal to 20°C and feed temperature varying from 45°C to 65°C. Therefore, the increase in the membrane thickness reduces the temperature polarization and offers more resistance to the mass transfer by decreasing the gradient of the partial water vapor pressure across the membrane. (ii) An increase in the feed temperature leads to an increase in the vapor flux. The feed temperature can be considered as one of the most important parameters that characterizes the performance of the membrane distillation. The feed temperature increases the permeate flow in an approximately linear manner. This happens because the vapor pressure of the water increases exponentially with the temperature, as described by the Antoine equation.

4.3. Effect of the pore size on the permeate flux

The obtained results related to pore size effect on the water vapor flux is shown in Fig. 8. Results were presented for constant permeate temperature equal to T_c = 20°C and constant feed temperature equal to T_h = 60°C. As illustrated, the rise of the pore diameter from d_p = 0.2 μm to d_p = 0.5 μm increases the permeate flux by a factor of 0.4% for the both cases of membrane thickness (δ = 100 μm and δ = 200 μm). The larger the pore size is, the more important the gas quantity driven by pressure gradient across the membrane. This behavior may exert on permeate flux. Therefore, the total vapor flux across the membrane can be estimated by summing the water vapor over the entire system of pores.

Fig. 8 shows that the membrane pore size does not have a great effect on the permeate flux. For these conditions it seems that the pore size d_p = 0.2 μm is the critical value of the pore diameter where the permeate flux remains constant as studied by Lawal and Khalifa [13].

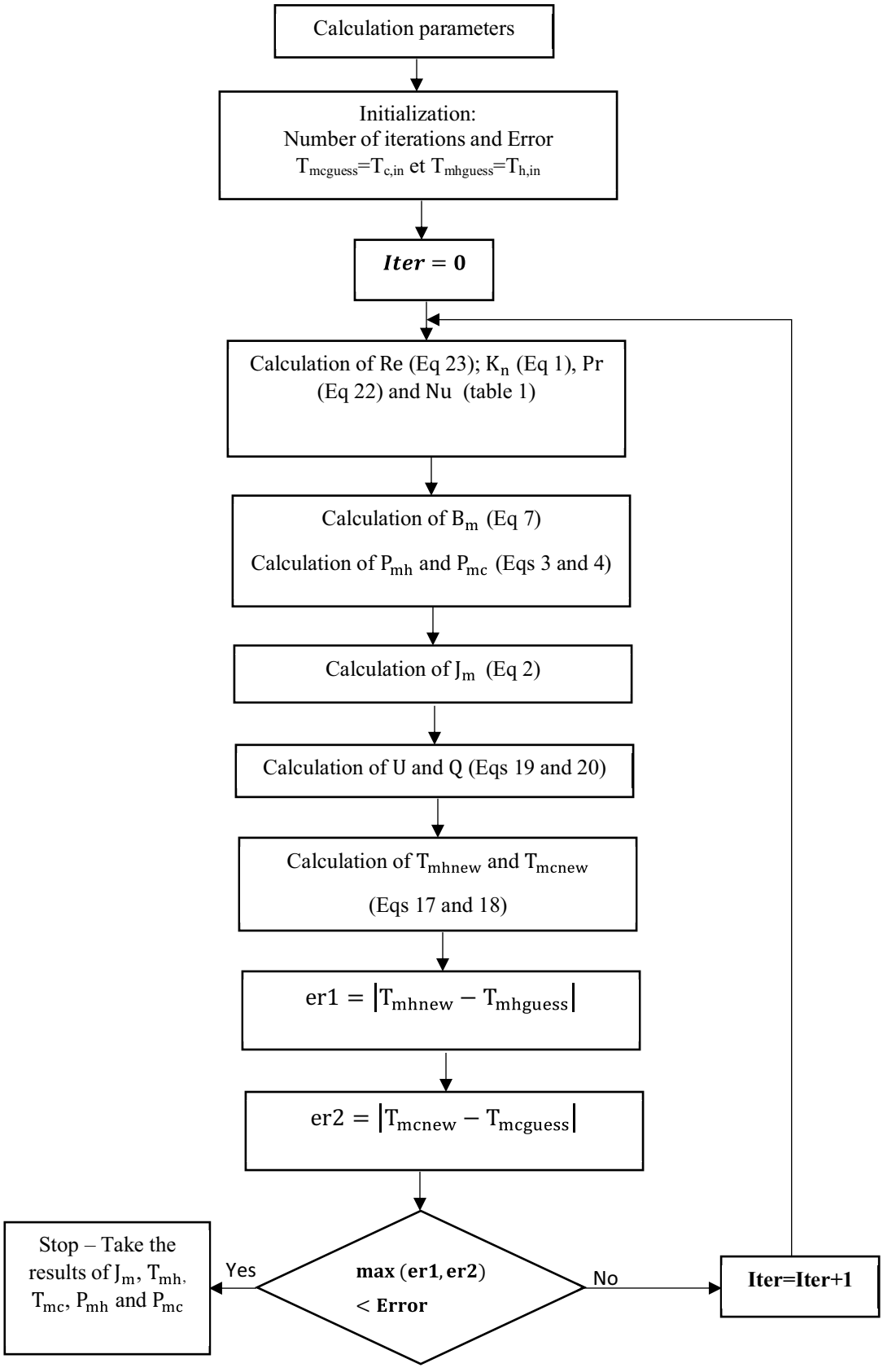

Fig. 2. Calculation flowchart.

Table 3
Membrane characteristics and geometry [12]

Symbols	Values as used in our code and Andrjesdóttir et al. [12] experiments
δ	160 μm
ε	0.88
K_g	0.029 W mK^{-1}
K_p	0.259 W mK^{-1}
d_p	0.2 μm
A	11.7 × 10^{-3} m^2
d_h	5.2 × 10^{-3} m

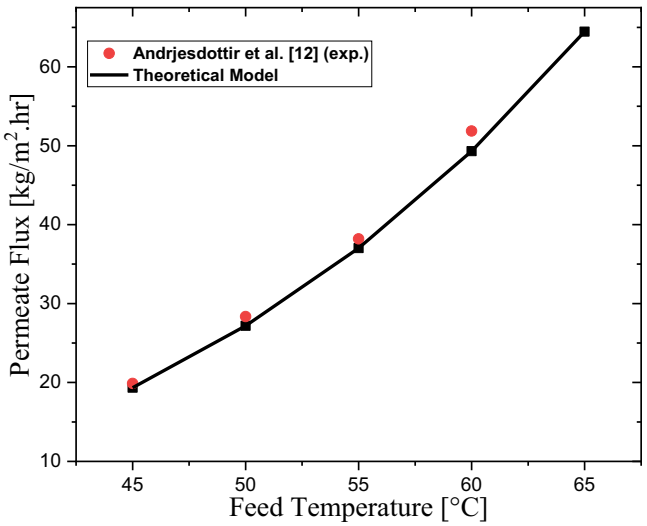

Fig. 3. Validation of the model results.

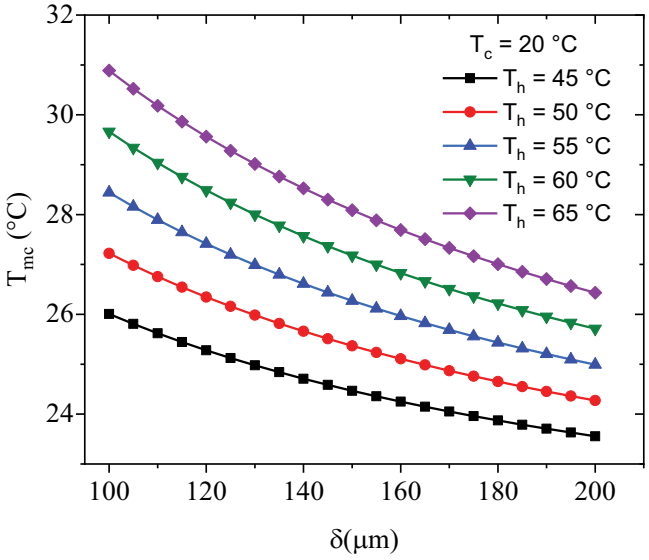

Fig. 4. Effect of the membrane thickness on the temperature of the permeate-membrane interface.

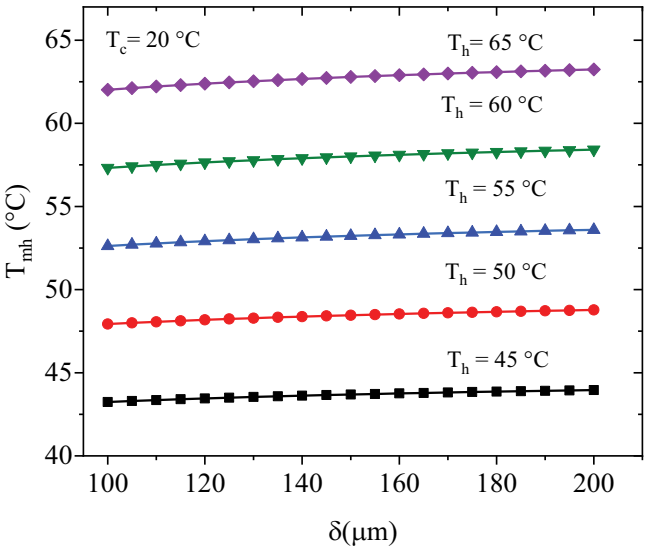

Fig. 5. Effect of the membrane thickness on the temperature of the feed-membrane interface.

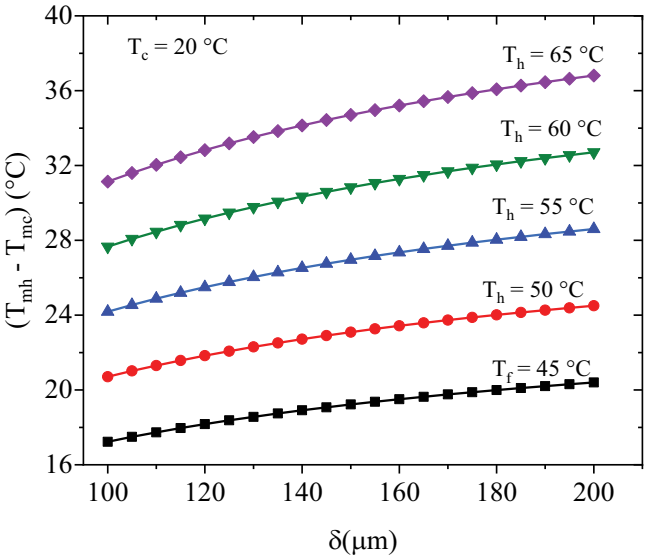

Fig. 6. Effect of the membrane thickness on the temperature difference through the membrane interfaces.

4.4. Effect of the porosity on the permeate flux

The obtained results of the membrane porosity effect on the water vapor flux are shown in Fig. 9. Results were presented for constant permeate temperature equal to T_c = 20°C and constant feed temperature equal to T_h = 60°C. As illustrated, the rise in the membrane porosity from ε = 70% to ε = 96%, increases the water vapor flux from 27 to 45 kg m^{-2} h^{-1} for δ = 100 μm and from 48 to 80 kg m^{-2} h^{-1} for δ = 200 μm, that gives an increase by a same amount equal to 40%.

High porosity reduces the thermal conductivity and increases the permeability of the membrane, which results in rise in permeate flux and heat efficiency. However, higher porosity means more pore channels are opened for

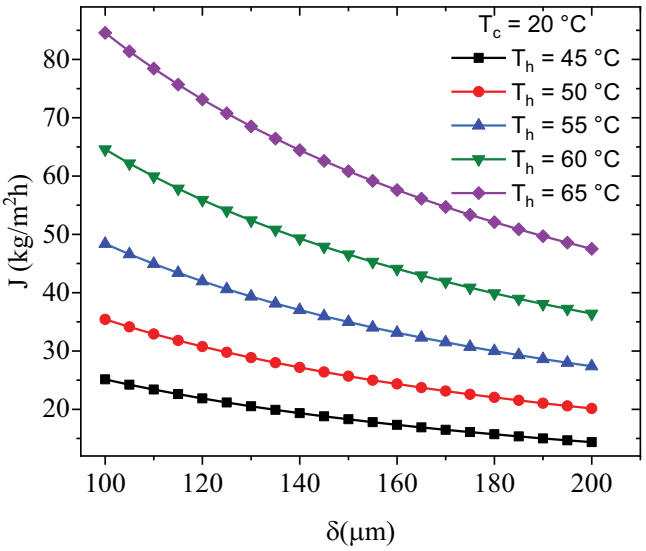

Fig. 7. Effect of the membrane thickness on the permeate flux.

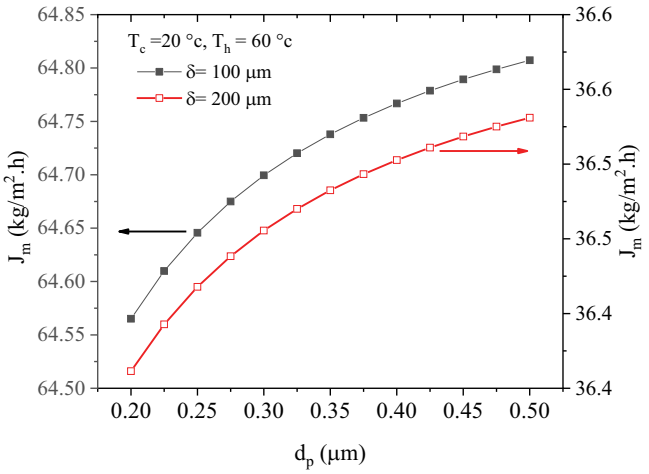

Fig. 8. Effect of the pore diameter on the permeate flux.

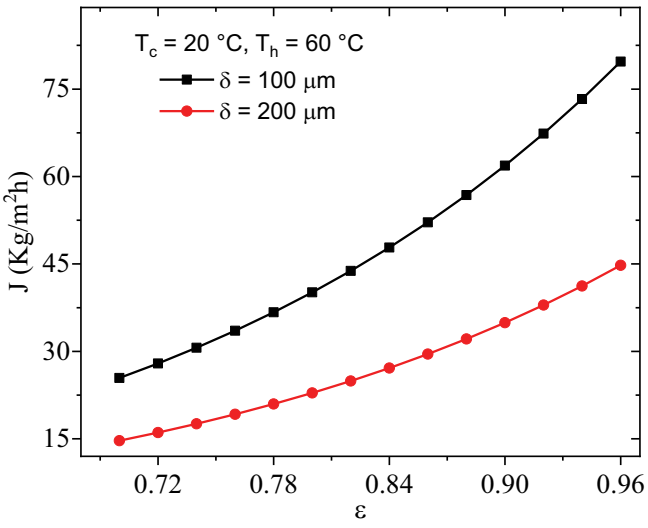

Fig. 9. Effect of the porosity on the permeate flux.

diffusion, hence higher permeate flux. This is because higher porosity decreases the heat effect loss by conduction

4.5. Effect of the membrane length on the permeate flux

The effects of the membrane length on vapor flux are depicted in Fig. 10. Results were presented for constant permeate temperature equal to T_c = 20°C, constant feed temperature equal to T_h = 60°C, δ = 100 μm and d_p = 0.2 μm. As illustrated, an increase of the membrane length from 0.12 to 0.4 m reduces the flux of permeate by 9% (for ε = 70%) and 7.7% (for ε = 90%). Temperature polarization increases with membrane length. When the contact area increases, the total exchanged heat between the feed and permeate section increases too. It results in the reduction of the temperature at the feed-membrane interface and rise in temperature at the permeate membrane interface. Consequently, the driving force of the process is decreasing (Fig. 11).

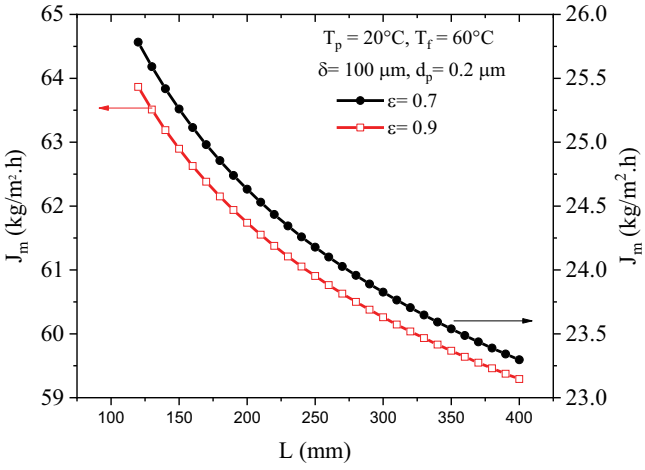

Fig. 10. Effect of the membrane length on the permeate flux.

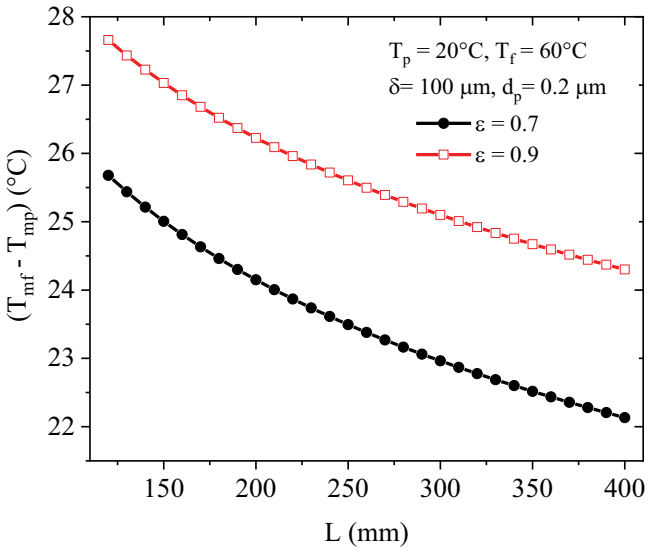

Fig. 11. Effect of the membrane length on the driving force of the process.

It is shown that a rise of the membrane length from 0.12 to 0.4 m decreases the interface temperatures difference ($T_{mh} - T_{mc}$) by 13.8% (for ε = 70%) and 12.1% (for ε = 90%).

5. Conclusion

Theoretical DCMD performance studies were conducted for different membrane characteristics. Simulations studies have been achieved, at constant permeate temperature and for various feed inlet temperatures, to grasp the effects on permeate flux and membrane performance.

A theoretical model was developed for performance modelling of one membrane layer used in direct contact membrane distillation. Regarding membranes, it was shown that having higher porosity and being thinner was important for higher permeate flux. Permeate flux, at optimal porosity and membrane thickness, was less sensitive to pore size variation.

Results showed that permeate flux decreased by a value of 43% with the increase of the membrane thickness from 100 to 200 μm. Results also revealed that the rise in the membrane porosity from ε = 70% to ε = 96%, increases the permeate by a value of 40%.

Successful attempt for modelling one membrane layer used in direct contact membrane distillation can lead to in-depth analysis of heat and mass transfer phenomena for the membranes.

Symbols

B_m	—	Mass transfer coefficient, kg m^{-2} h^{-1} Pa^{-1}
C_p	—	Specific heat of water, J kg^{-1} K^{-1}
d_h	—	Hydraulic diameter, m
d_p	—	Mean pore diameter of the membrane, m
h_c	—	Heat transfer coefficient of permeate, W m^{-2} K^{-1}
h_h	—	Heat transfer coefficient of feed, W m^{-2} K^{-1}
h_m	—	Heat transfer coefficient of the membrane, W m^{-2} K^{-1}
J_m	—	Permeate flux, kg m^{-2} h^{-1}
K_B	—	Boltzmann constant (1.381 × 10^{-23}), J K^{-1}
K_g	—	Thermal conductivity of the gas filling the membrane pores, W m^{-1} K^{-1}
K_i	—	Mean thermal conductivity, W m^{-1} K^{-1}
K_m	—	Thermal conductivity of the membrane, W m^{-1} K^{-1}
Kn	—	Knudsen number, dimensionless
K_p	—	Thermal conductivity of the polymer, W m^{-1} K^{-1}
L_v	—	Heat of vaporization, J kg^{-1}
M_w	—	Molecular weight of water, g mol^{-1}
Nu	—	Nusselt number, Dimensionless
P_a	—	Air pressure inside the membrane pores, Pa
P.D	—	Diffusion coefficient in the pores, Pa m^2 s^{-1}
P_{mc}	—	Membrane interface partial pressure of water molecule on the permeate side, Pa
P_{mh}	—	Membrane interface partial pressure of water molecule on the feed side, Pa
Pr	—	Prandtl number, dimensionless
R	—	Universal gas constant, 8.314472 J mol^{-1} K^{-1}
R_e	—	Reynolds number, dimensionless
T_c	—	Permeate temperature, °C
T_h	—	Feed temperature, °C
T_{mc}	—	Membrane interface temperature on permeate side, °C
T_{mh}	—	Membrane interface temperature on feed side, °C
T_{mav}	—	Mean temperature, $T_{mav} = (T_h + T_c)/2)$ (°C)
T_{mav}	—	Absolute mean temperature, °C
U	—	Overall heat transfer coefficient, W m^{-2} K^{-1}
v	—	Average velocity, m s^{-1}
α	—	Thermal diffusivity, m^2 s^{-1}
δ	—	Membrane thickness, m
ε	—	Membrane porosity, %
μ	—	Dynamic viscosity, Pa s
ν	—	Kinematic viscosity, m^2 s^{-1}
ρ	—	Density, kg m^{-3}
τ	—	Membrane tortuosity

References

[1] R.W. Schofield, A.G. Fane, C.J.D. Fell, Heat and mass transfer in membrane distillation, J. Membr. Sci., 33 (1987) 299–313.

[2] R.W. Schofield, A.G. Fane, C.J.D. Fell, R. Macoun, Factors affecting flux in membrane distillation, Desalination, 77 (1990) 279–294.

[3] R.W. Schofield, A.G. Fane, C.J.D. Fell, Gas and vapour transport through microporous membranes. I. Knudsen-Poiseuille transition, J. Membr. Sci., 53 (1990) 159–171.

[4] M. Tomaszewska, M. Gryta, A.W. Morawski, A study of separation by the direct-contact membrane distillation process, Sep. Technol., 4 (1994) 244–248.

[5] F. Laganà, G. Barbieri, E. Drioli, Direct contact membrane distillation: modelling and concentration experiments, J. Membr. Sci., 166 (2000) 1–11.

[6] Z. Ding, R. Ma, A.G. Fane, A new model for mass transfer in direct contact membrane distillation, Desalination, 151 (2003) 217–227.

[7] J. Phattaranawik, R. Jiraratananon, A.G. Fane: Heat transport and membrane distillation coefficients in direct contact membrane distillation, J. Membr. Sci., 212 (2003) 177–193.

[8] Y. Yuna, R. Ma, W. Zhang, A.G. Fane, J. Li, Direct contact membrane distillation mechanism for high concentration NaCl solutions, Desalination, 188 (2006) 251–262.

[9] M. Qtaishat, T. Matsuura, B. Kruczek, M. Khayet, Heat and mass transfer analysis in direct contact membrane distillation, Desalination, 219 (2008) 272–292.

[10] H. Yu, X. Yang, R. Wang, A.G. Fane, Analysis of heat and mass transfer by CFD for performance enhancement in direct contact membrane distillation, J. Membr. Sci., 405–406 (2012) 38–47.

[11] X. Yang, H. Yu, R. Wang, A.G. Fane, Optimization of microstructured hollow fiber design for membrane distillation applications using CFD modeling, J. Membr. Sci., 421–422 (2012) 258–270.

[12] Ó. Andrjesdóttir, C.L. Ong, M. Nabavi, S. Paredes, A.S.G. Khalil, B. Michel, D. Poulikakos, An experimentally optimized model for heat and mass transfer in direct contact membrane distillation, Int. J. Heat Mass Transfer, 66 (2013) 855–867.

[13] D.U. Lawal, A.E. Khalifa, Flux prediction in direct contact membrane distillation, Int. J. Mater. Mech. Manuf., 2 (2014) 302–308.

[14] H. Hayer, O. Bakhtiari, T. Mohammadi, Simulation of momentum, heat and mass transfer in direct contact membrane distillation: a computational fluid dynamics approach, J. Ind. Eng. Chem., 21 (2015) 1379–1382.

[15] R. Bouchrit, A. Boubakri, A. Hafiane, S. Al-Tahar Bouguecha, Direct contact membrane distillation: capability to treat hypersaline solution, Desalination, 376 (2015) 117–129.

[16] R.D. Gustafson, J.R. Murphy, A. Achilli, A stepwise model of direct contact membrane distillation for application to large-scale systems: experimental results and model predictions, Desalination, 378 (2016) 14–27.
[17] F. Eleiwi, N. Ghaffour, A.S. Alsaadi, L. Francis, T.M. Laleg-Kirati, Dynamic modeling and experimental validation for direct contact membrane distillation (DCMD) process, Desalination, 384 (2016) 1–11.
[18] D. Cheng, W. Gong, N. Li, Response surface modeling and optimization of direct contact membrane distillation for water desalination, Desalination, 394 (2016) 108–122.
[19] D.K. Patil, Dr. Sanjay P. Shirsat, Membrane distillation review and flux prediction in direct contact membrane distillation process, Int. Res. J. Eng. Technol. (IRJET), 4 (2017) 829–845.
[20] A. Ali, J.-H. Tsai, K.-L. Tung, E. Drioli, F. Macedonio, Designing and optimization of continuous direct contact membrane distillation process, Desalination, 426 (2018) 97–107.
[21] E. Ali, J. Orfi, An experimentally calibrated model for heat and mass transfer in full-scale direct contact membrane distillation, Desal. Water Treat., 116 (2018) 1–18.
[22] J. Lou, J. Vanneste, S.C. DeCaluwe, T.Y. Cath, N. Tilton, Computational fluid dynamics simulations of polarization phenomena in direct contact membrane distillation, J. Membr. Sci., 591 (2019) 1–18.
[23] W. Ni, Y. Li, J. Zhao, G. Zhang, X. Du, Y. Dong, Simulation study on direct contact membrane distillation modules for high-concentration NaCl solution, Membranes, 10 (2020) 1–18.
[24] U.F. Alqsair, A.M. Alwatban, A. Oztekin, A.M. Alshwairekh, R. Krysko, Comparison of Sweeping Gas and Direct Contact Membrane Distillation – Module Length Effect, Proceedings of the ASME 2020 Summer Heat Transfer Conference (SHTC2020), Rosen Shingle Creek, FL, USA, 2020, pp. 1–9.
[25] N.A. Mohammad Ameen, S.S. Ibrahim, Q.F. Alsalhy, A. Figoli, Highly saline water desalination using direct contact membrane distillation (DCMD): experimental and simulation study, Water, 12 (2020) 1–24.
[26] Q.L. Ve, R. Koirala, M. Bawahab, H. Faqeha, M.C. Do, Q.L. Nguyen, A. Date, A. Akbarzadeh, Experimental investigation of the effect of the spacer and operating conditions on mass transfer in direct contact membrane distillation, Desalination, 500 (2021) 1–24.
[27] E.N. Sieder, G.E. Tate: Heat transfer and pressure drop of liquid in tubes, Ind. Eng. Chem., 28 (1936) 1429–1435.
[28] L.C. Thomas, Heat Transfer, Prentice-Hall, Englewood Cliffs, NJ, 1992.
[29] A.K. Coker, Ludwig's Applied Process Design for Chemical and Petrochemical Plants, Gulf Professional Publishing, Oxford, UK, 2014.
[30] J. Zhang, Theoretical and Experimental Investigation of Membrane Distillation, School of Engineering & Science, Ph.D. Thesis, Victoria University, Melbourne, Australia, 2011.